Journal of Catalysis 260 (2008) 254–261

Contents lists available at ScienceDirect

Journal of Catalysis

www.elsevier.com/locate/jcat

Mechanistic pathway for methane formation over an iron-based catalyst

Nilenindran S. Govender [a], F. Gideon Botes [b], Mart H.J.M. de Croon [a], Jaap C. Schouten [a,*]

[a] Laboratory of Chemical Reactor Engineering, Department of Chemical Engineering & Chemistry, Eindhoven University of Technology, P.O. Box 513, 5600 MB Eindhoven, The Netherlands
[b] Sasol Technology R&D (Pty) Ltd, P.O. Box 1, Sasolburg, 1947, South Africa

ARTICLE INFO

Article history:
Received 29 August 2008
Accepted 3 October 2008
Available online 5 November 2008

Keywords:
SSITKA
Methanation
Fischer–Tropsch
Iron catalyst
Reaction mechanism
Transient kinetic model
Parameter estimation

ABSTRACT

The methanation reaction mechanism under Fischer–Tropsch conditions is investigated with the Steady State Isotopic Transient Kinetic Analysis (SSITKA) technique over a precipitated iron-based catalyst. The $^{13}CH_4$ transients resulting from a $^{12}CO \rightarrow {}^{13}CO$ switch (330 °C, 1.2 bar, and $H_2/CO = 15$) provided kinetic information for the methanation reaction. Six methanation models were screened and only three of these could describe the methane transient. These models were subsequently extended to account for the Fischer–Tropsch higher hydrocarbon products by considering C–C coupling reactions and the kinetic rate parameters were estimated. The result was two indistinguishable mechanisms which could describe the methane transient as well as the experimental steady-state concentrations. Both mechanisms have two active pools of carbon (C_α and C_β) on the catalyst surface with both leading towards the formation of methane. The C_β pool is 25 to 50 times less active than the C_α pool for methanation and occupies 92% of the total CH_x coverage (0.25 ML). The C–C coupling reaction was shown to involve both the C_α and C_β pools. The concentration of molecularly adsorbed CO on the Fe-based catalyst is shown to be extremely low, with an estimated surface coverage of 9×10^{-4} ML.

1. Introduction

The Fischer–Tropsch synthesis (FTS) is a heterogeneously catalysed process whereby synthesis gas (a mixture of carbon monoxide and hydrogen) is converted to liquid fuels (gasoline and diesel) and chemicals [1]. Dry [2] describes two modes of operation for the Fischer–Tropsch synthesis, each with its specific selectivity targets. The high temperature (300–350 °C) Fischer–Tropsch process (HTFT) aims at the production of gasoline and linear low molecular mass olefins, whereas the low temperature (200–240 °C) Fischer–Tropsch process (LTFT) is used for the production of diesel and high molecular mass linear waxes. Sasol's commercial HTFT and LTFT processes are described briefly by Steynberg et al. [3] and Espinoza et al. [4], respectively, whilst details of the entire FTS have recently been published by Steynberg [5]. The HTFT process comprises a complex network of elementary reaction steps. Apart from the usual linear FT products (olefins and paraffins), these steps include the formation of CO_2, carbon, and oxygenates (alcohols, acids, aldehydes and ketones). To date, the product distribution of the HTFT process has not been fully described by the mechanisms in the literature. Kinetic equations proposed for this process have either been developed empirically or based on a mechanism, using a postulated rate determining step. Hence these expressions do not illustrate a uniform picture.

The steady-state isotopic transient kinetic analysis (SSITKA) technique was developed by Happel [6], Bennett [7] and Biloen [8], to obtain *in situ* kinetic information about reaction mechanisms and reaction intermediates on the catalyst surface. An extensive review of the SSITKA methodology is given by Shannon and Goodwin [9]. In a nutshell, this technique keeps the catalyst under steady-state conditions and introduces an isotopic transient by abruptly replacing one reactant with its isotope. For example, a feed of $H_2/{}^{12}CO/Ar$ is switched to $H_2/{}^{13}CO/He$ with minimum disturbance to the system. The inert gas is also switched to determine the gas hold-up in the reactor. Apart from isothermal and isobaric reactor conditions, the surface composition of the catalyst does not change during SSITKA, making this technique ideal for reaction mechanistic studies. The methanation reaction has proven to be an ideal system for isotopic transient kinetic investigations due to the simple molecules involved, which are easy to trace by mass spectrometry (MS). A study of this reaction under FT conditions would be useful in developing a complete kinetic framework which could also be used to formulate more robust steady-state kinetic models. It is reasonable to assume that methane is formed by the stepwise hydrogenation of C atoms producing CH_x ($x = 1$ to 3) groups. For iron catalysts, there is still uncertainty about the abundance and nature of the surface species and the rate limiting step of the surface reactions. One reason for this is that iron forms several different types of surface carbides [10,11], some of which have been shown to be active for FTS. These key questions regard-

* Corresponding author.
E-mail address: j.c.schouten@tue.nl (J.C. Schouten).

0021-9517/$ – see front matter
doi:10.1016/j.jcat.2008.10.008

ing iron catalysts have been addressed by several authors also for other FT active metal (Rh, Ru, Co and Ni) catalysts.

High CO coverage, in some cases near a monolayer, has been reported by Efstathiou et al. [12–16] and Siddall et al. [17] over Rh-based catalysts, Agnelli et al. [18] over Ni catalysts, Bajusz and Goodwin [19] for Ru-based catalysts, and Van Dijk et al. [20] for Co-based catalysts. In all of these studies, the coverage of CO was reported to be higher than the monomeric building units (CH_x). The authors of this paper are not aware of any reports in the literature for such high CO coverage on Fe-based catalysts. Mims and McCandish [21,22] performed SSITKA experiments on a promoted Fe catalyst at 237 °C, $H_2/CO = 1$, and 1 bar. There was no measurable delay between the Ar and ^{13}CO transients, implying extremely low CO coverage. Stockwell et al. [23] studied the mechanism of methane and hydrocarbon formation on a 10 wt% Fe/Al_2O_3 catalyst using ^{12}CO to ^{13}CO SSITKA. The amount of $^{12}CO_{ads}$ measured was very small, only 8 μmol CO_{ads}/g_{cat} equivalent to 0.1 monolayer of CO after 1.5 h on stream at 285 °C, $H_2/CO = 9$, 1 bar, and 7% conversion to Fischer–Tropsch products.

The rate of CO dissociation was reported to be rate determining by both Efstathiou et al. [12–16] and Siddall et al. [17] over Rh-based catalysts, whilst for a similar catalyst, Balakos et al. [24] reported that hydrogenation of CH_x is the rate determining step. Stockwell et al. [25] on the other hand could not distinguish between these two rates on a Ni-based catalyst and concluded that both are kinetically important. More specifically, Van Dijk et al. [20] concluded that the $C_{ads} \rightarrow CH_{ads}$ reaction step was the rate determining step for their Co-based catalyst, whilst Mirodatos et al. [18,26] showed that the CH into CH_2 step was rate determining using both ^{13}CO and D_2 tracing on a Ni/SiO_2 catalyst. There is uncertainty as to which elementary reaction step is rate determining during methanation. For Fe catalysts, such information obtained from transient studies has not been published.

The most abundant CH_x surface species was identified as CH_{ads} by Happel et al. [27] on a Ni-based catalyst. For a Co-based catalyst, Van Dijk et al. [20] identified C_{ads} as the most abundant methane intermediate. Krishna and Bell [28] studied chain growth during FTS over Ru/TiO_2 using ^{13}CO and D_2 tracing. They concluded that the dominant species are monomeric building units (0.2 to 0.6 ML), whilst growing alkyl chains occupy less than 0.2 ML and CO_{ads} occupied an additional 0.7 ML. There are no transient studies reporting the nature of the surface species on Fe catalysts.

Two parallel pools of surface intermediates, $C_\alpha H_x$ and $C_\beta H_x$ are proposed by Balakos [24] to react irreversibly to CH_4 on a 3 wt% Rh/SiO_2 catalyst. Happel et al. [27,29–31] showed that carbidic carbon consists of two pools, a smaller active C_{ads} pool and a larger methanation inactive C pool which is not graphitic. More than a decade later [31], they showed that the data in the aforementioned studies could be modeled using a mechanism consisting of two parallel paths, where both paths lead independently to the formation of methane. Bajusz and Goodwin [19] also identified two active pools (C_α and C_β) which can be hydrogenated to methane. Both Van Dijk et al. [20] and Soong et al. [32] modeled such a pathway for a Co-based and a Raney-nickel catalyst, respectively.

The purpose of this work is to develop a plausible mechanism for the methanation reaction under HTFT conditions for an Fe-based catalysts using SSITKA. Our approach is to model the ^{13}CO and $^{13}CH_4$ transients obtained from a $^{12}CO \rightarrow {}^{13}CO$ SSITKA experiment and then to use parameter estimation to discriminate between several rival models. There are no such studies to date reported in the open literature.

2. Experimental

2.1. Catalyst preparation

The Fe catalyst was prepared by co-precipitation of metal nitrates as described by Espinoza et al. [33]. The catalyst used in this study was supplied by Sasol Technology Research and Development and contains only potassium as a promoter. The exact composition is not mentioned due to confidentiality. The surface area of the unreduced catalyst measured by N_2 physisorption is 27 $m^2\,g_{cat}^{-1}$, which is in the range specified by Espinoza et al. [33] for this type of Fe-based catalyst.

2.2. Catalyst pretreatment, activation, and FT synthesis

Typically 0.5–1.0 g of Fe/K catalyst is weighed and mixed with 1.0–2.5 g of SiC to create the catalyst bed. The catalyst is reduced with 50 vol% H_2/Ar mixture (total flow of 80 ml min^{-1}) at 420 °C and 1.2 bar for 16 h. After the reduction the reactor is cooled under an Ar flow down to the FT synthesis temperature of 330 °C. At this temperature, the synthesis is started by introducing H_2 and CO flows at the desired H_2/CO ratio and gas hourly space velocity (GHSV). The catalyst mass in certain experiments was varied to obtain a different GHSV.

2.3. Data analysis and treatment

2.3.1. Steady-state results

The steady state performance of the catalyst was monitored online by a Varian CP-3800 Gas Chromatograph consisting of one thermal conductivity detector (TCD) and two Flame Ionization detectors (FID). The unreacted feed and some hydrocarbon products (N_2, H_2, CO, CO_2, and CH_4) were analysed by the TCD, whilst C_1 to C_5 hydrocarbons was analysed by the FID.

2.3.2. Transients using the online mass spectrometer

A Balzers ThermoStar™ (GSD 301T) mass spectrometer was used to monitor the reactants (H_2 and CO), inerts (Ar and Ne), and small molecular weight products (for example CH_4 and CO_2). The m/e values used in our experiments were 2, 15, 17, 22, 28, 29, 40, 44, and 45 for H_2, $^{12}CH_4$, $^{13}CH_4$, Ne, ^{12}CO, ^{13}CO, Ar, $^{12}CO_2$, and $^{13}CO_2$. The transient responses are normalised between the initial MS intensity before the isotopic step change and the final MS intensity at the moment in time when the unlabeled atom in all surface and gas phase species is replaced by its labeled counterpart, as shown in Eq. (1) in the case of the inert Ne:

$$I_{Ne,N} = \frac{I_{Ne,t} - I_{Ne,max}}{I_{Ne,max} - I_{Ne,min}}, \tag{1}$$

where $I_{Ne,N}$ is the normalised transient of Ne, $I_{Ne,t}$ is the MS intensity of Ne, $I_{Ne,max}$ is the maximum MS intensity of Ne, and $I_{Ne,min}$ is the minimum MS intensity of Ne.

2.3.3. Reactor modeling

Happel [34] and Bennet et al. [35] showed that SSITKA experiments are optimal in plug flow reactors due to the fast isotopic step change. In a plug flow regime, all changes relative to the inlet signal are ascribed to kinetics. The fixed-bed reactor used in this study is modeled as an isothermal and isobaric plug flow reactor. The total molar flow rate throughout the catalyst bed is assumed constant due to the low conversions.

Mass balances for only the labeled gaseous and surface species, represented by partial differential equations in time and space, are solved. The continuity equations for the labeled gaseous component $X^\#$ and the surface component $Y^\#$ are as follows:

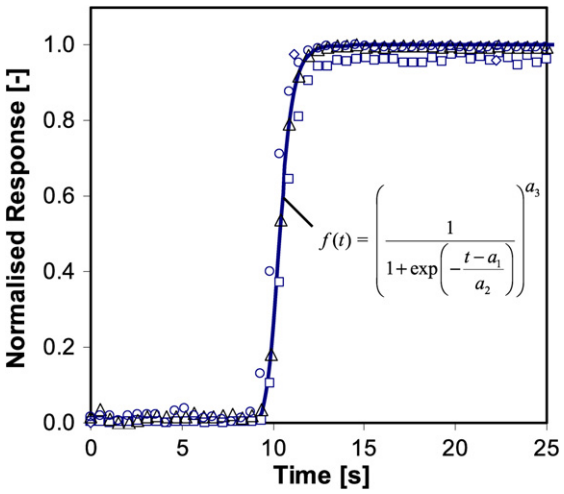

Fig. 1. The optimal fit for the empirical function used in this study. The open markers (○, △, and □) are Ne data collected at $H_2/CO = 15$, 330 °C, 1.2 bar, and GHSV = 7412 ml h^{-1} g_{cat}^{-1}. The solid line is the optimal fit with $a_1 = 9.01$, $a_2 = 0.52$, and $a_3 = 10.81$.

$$\frac{\partial C_{X^\#}}{\partial t} + \frac{1}{\tau}\frac{\partial C_{X^\#}}{\partial x} = \frac{\rho}{\varepsilon_b} R_{W,X^\#}, \tag{2}$$

$$\frac{\partial L_{Y^\#}}{\partial t} = R_{W,Y^\#}. \tag{3}$$

The initial and boundary conditions for an isotopic step from gas-phase reactant Z to $Z^\#$ are as follows.

Initial conditions:

$$t = 0, \quad C_{X^\#} = L_{Y^\#} = 0, \text{ for any } x.$$

Boundary conditions:

$$t > 0, \quad x = 0, \quad C_{Z^\#} = \text{input function}, f(t),$$

$$t > 0, \quad x = 0, \quad C_{X^\#} = 0, \text{ for } X^\# \neq Z^\#, \tag{4}$$

where C_X (mol m_g^{-3}) is the concentration of component X in the gas phase; L_Y (mol kg_{cat}^{-1}) is the surface concentration of Y; τ (s) is the residence time; t (s) is the time; ρ_b (kg_{cat} m_b^{-3}) is the density of the catalyst bed; ε_b (m_g^3 m_b^{-3}) is the catalyst bed porosity; $R_{W,X^\#}$ (mol kg_{cat}^{-1} s^{-1}) is the steady state production rate of X; x is the dimensionless axial position in the catalyst bed.

The residence time τ can be calculated as:

$$\tau = \frac{\varepsilon_b V_R}{F_V}, \tag{5}$$

where V_R (m_b^3) is the volume of the catalyst bed and F_V (m_g^3 s^{-1}) is the total volumetric flow rate at reaction temperature and pressure. The input function $f(t)$ is represented by the transient of the inert tracer. The optimal fit for the empirical input function used in this work is shown in Fig. 1.

2.3.4. Parameter estimation

The set of partial Differential Equations (Eqs. (2) and (3)) with its initial and boundary conditions (Eq. (4)) is solved using the software package gPROMS (general PROcess Modeling System). Parameter estimation in gPROMS [36] uses a maximum likelihood objective function (Eq. (6)) in which Φ is the objective function, N is the total number of measurements taken in all experiments, θ is the set of model parameters to be estimated, NE is the number of performed experiments, NV_i is the number of variables measured in experiment i, NM_{ij} is the number of measurements of variable j in experiment i, σ_{ijk}^2 is the variance of the kth measurement of variable j in experiment i, $\tilde{z}_{ijk}$ is the experimental value for the kth measurement of variable j in experiment i, and z_{ijk} is the model prediction for the kth measurement of variable j in experiment i

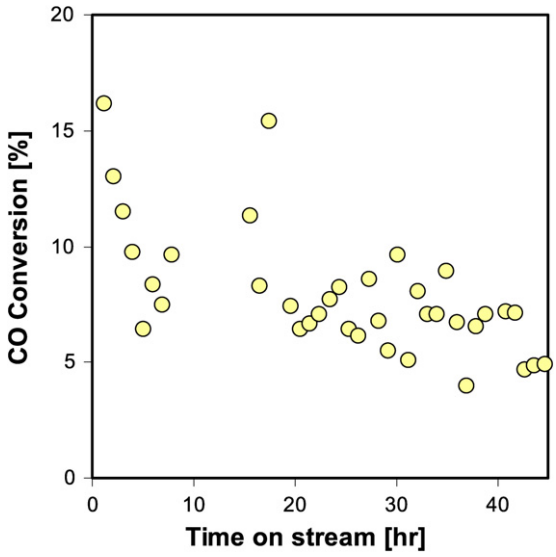

Fig. 2. CO conversion data obtained at $H_2/CO = 15$, 330 °C, 1.2 bar, and GHSV = 7412 ml h^{-1} g_{cat}^{-1}.

$$\Phi = \frac{N}{2}\ln(2\pi) + \frac{1}{2}\min_\theta \left\{ \sum_{i=1}^{NE}\sum_{j=1}^{NV_i}\sum_{k=1}^{NM_{ij}} \left[\ln\left(\sigma_{ijk}^2\right) + \frac{(\tilde{z}_{ijk} - z_{ijk})^2}{\sigma_{ijk}^2} \right] \right\}. \tag{6}$$

The principle of parameter estimation is based upon the minimization of the difference between the experimental values and the model predicted values (Eq. (7)), in which ξ_i is the difference between experimental and predicted value for measurement i, $\tilde{z}_i$ is the experimental value for measurement i, and $z_i(\theta)$ is the predicted value for measurement i

$$\xi_i = \tilde{z}_i - z_i(\theta). \tag{7}$$

The maximum likelihood principle assumes ξ_i to be independent and normally distributed with zero mean and standard deviation σ_i. Several variance models that can describe the standard deviation for ξ_i are available in gPROMS. The constant variance model in which the measurement error has a constant standard deviation is used in our study.

3. Results and discussion

3.1. Steady state results

Both the catalyst and the reaction should be at steady state before performing a SSITKA experiment. Steady state was monitored online by calculating the CO conversion. The data for one of our runs in Fig. 2 shows that there is a sharp decline in the CO conversion in the first 10 h exposure to synthesis gas. This is attributed to the changes in the catalyst morphology. Dry [37] showed that during this induction period, the iron catalyst changes from iron oxide and iron to mostly iron carbides. Du Plessis [38] observed the same high CO conversion in the first 5 to 10 h for potassium promoted iron catalyst under HTFT conditions and used *in situ* XRD to show that this initial change in activity is due to the formation and stability of the various iron carbides. It is safe to assume, based on the aforementioned study and our data, that minimal changes to the catalyst occur after the first 10 h of operation. Most of our SSITKA experiments were performed after 20 h exposure to synthesis gas. To avoid excessive carbon formation, the synthesis was stopped overnight and re-started the following morning.

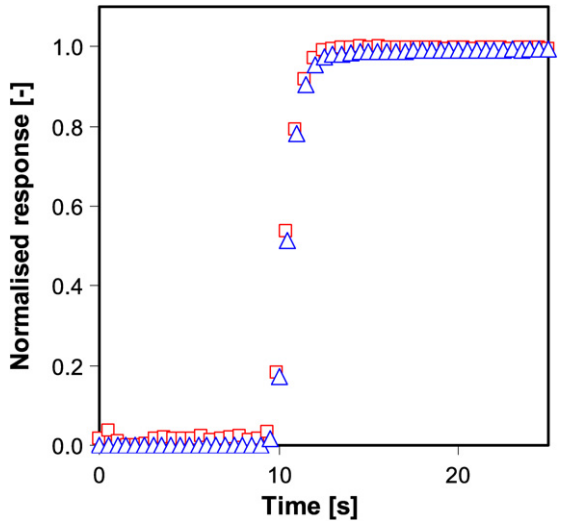

Fig. 3. Normalised transient responses for ^{13}CO (○) and Ne (□) obtained at $H_2/CO = 15$, 330 °C, 1.2 bar, and GHSV = 7412 ml h^{-1} g_{cat}^{-1}. For clarity reasons, data from only one run is shown.

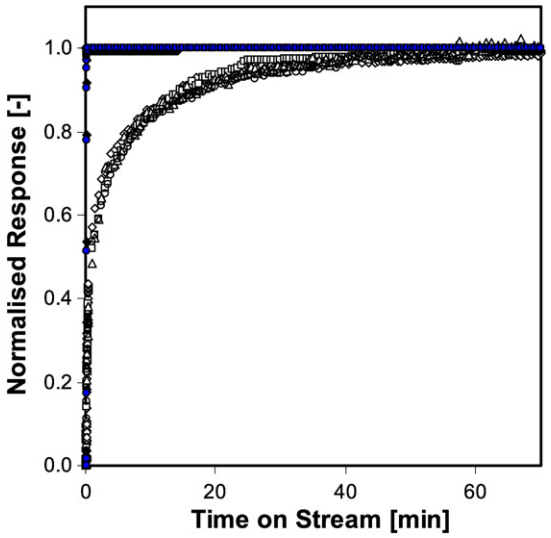

Fig. 4. Normalised transient responses for ^{13}CO (◆), Ne (●) and $^{13}CH_4$ (○, □, △, and ◇) obtained at $H_2/CO = 15$, 330 °C, 1.2 bar, and GHSV = 7412 ml h^{-1} g_{cat}^{-1}.

Typically, the catalyst undergoes a quick re-activation (shown in Fig. 2 at 15 h) and then reaches the same steady state CO conversion.

3.2. SSITKA results

A delay on the ^{13}CO response is usually observed with $^{12}CO \rightarrow {}^{13}CO$ SSITKA experiments which results from the time required for the ^{13}CO to replace the reservoir of $^{12}CO_{ads}$. This phenomenon is commonly referred to as the chromatographic effect [9,34,39]. The absence of this chromatographic effect in our results, shown in Fig. 3, suggests an extremely low surface coverage of CO_{ads}. The breakthrough of ^{13}CO is extremely fast and in all cases overlaps the Ne signal. This is consistent with the results by Mims et al. [21,22], Saudsakorn et al. [40] and Stockwell et al. [23] obtained on other Fe-based catalysts using the same transient technique at LTFT conditions. It has also been well documented [41,42] that low temperatures (−80 °C) are required to accurately measure CO chemisorbed on iron catalysts because it readily dissociates at room temperature. We could only measure 37 $\mu mol_{CO}\, g_{cat}^{-1}$ at 25 °C corresponding to a coverage of 0.1 ML, based on a surface area of 16 $m^2\, g^{-1}$ obtained by N_2 physisorption. The surface concentration of CO_{ads} can also be calculated according to:

$$L_{CO} = \frac{\tau_{CO} F_{CO}}{W_{cat}} = \frac{F_{CO}}{W_{cat}} \int_{t=0}^{\infty} \left[E_{^{12}CO}(t) - E_{Ne}(t)\right] dt, \tag{8}$$

where L_{CO} is the surface concentration of CO_{ads} in mol kg_{cat}^{-1}; F_{CO} is the molar feed rate of CO in mol s^{-1}; τ_{CO} is the mean residence time of CO_{ads} in s; W_{cat} is the weight of catalyst in the reactor bed in kg_{cat}; $E_{^{12}CO}$ is the normalised transient of ^{12}CO; and E_{Ne} is the normalised transient of Ne. The surface concentration calculated in this way is independent of the reaction mechanism. The mean residence time could not be accurately determined because of the extremely low CO coverage. A maximum value of 0.05 s was used in our study which resulted in a surface concentration of 2.4×10^{-4} mol kg_{cat}^{-1} ($\sim 9 \times 10^{-4}$ ML). This amount of CO on our Fe-based catalyst is 32 times lower than that reported by Stockwell et al. [23]. This deviation can be best ascribed to the higher temperatures used in this study.

The $^{13}CH_4$ transients for different runs at the same experimental conditions are presented in Fig. 4. The $^{13}CH_4$ transients reached 100% marking after 45 min but 90% of this is observed in the first

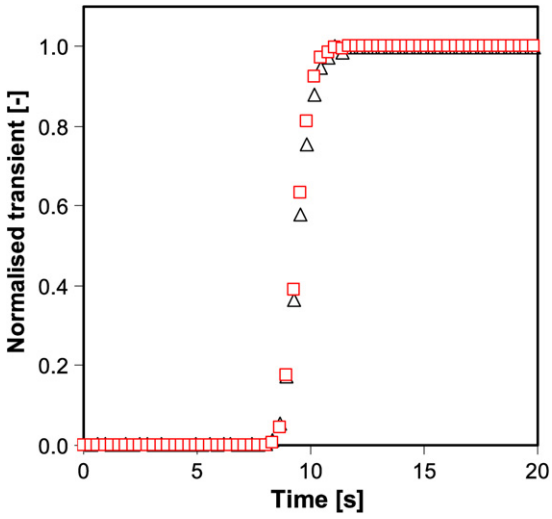

Fig. 5. Normalised transient responses for Ne (○) and $^{13}CH_4$ (□) obtained at 330 °C and 1.2 bar after a Ar → CH_4/Ne transient switch.

15 to 20 min. It seems that there are two distinct processes occurring; a fast route to methanation in the first few minutes and then a slower route which takes at least a further 30 min. The possibility that methane can readsorb and hence causes such a delay was also investigated. This was performed by using the transient switch, Ar → CH_4/Ne after the catalyst reached steady state and the reactor was purged with inert. The results (Fig. 5) show that there is no delay between the Ne and CH_4 transients confirming that methane does not readsorb onto the catalyst surface under our reaction conditions. The surface concentration of $C_{1,ads}$ can also be calculated from the transient data according to:

$$\begin{aligned} L_{C1} &= \frac{\tau_{C1} F_{CO} X_{CO}}{W_{cat}} \\ &= \frac{F_{CO}\, X_{CO}}{W_{cat}} \left(\int_{t=0}^{\infty} \left[E_{^{12}CH_4}(t) - E_{Ne}(t)\right] dt \right. \\ &\quad \left. - \frac{1}{2} \int_{t=0}^{\infty} \left[E_{^{12}CO}(t) - E_{Ne}(t)\right] dt \right), \end{aligned} \tag{9}$$

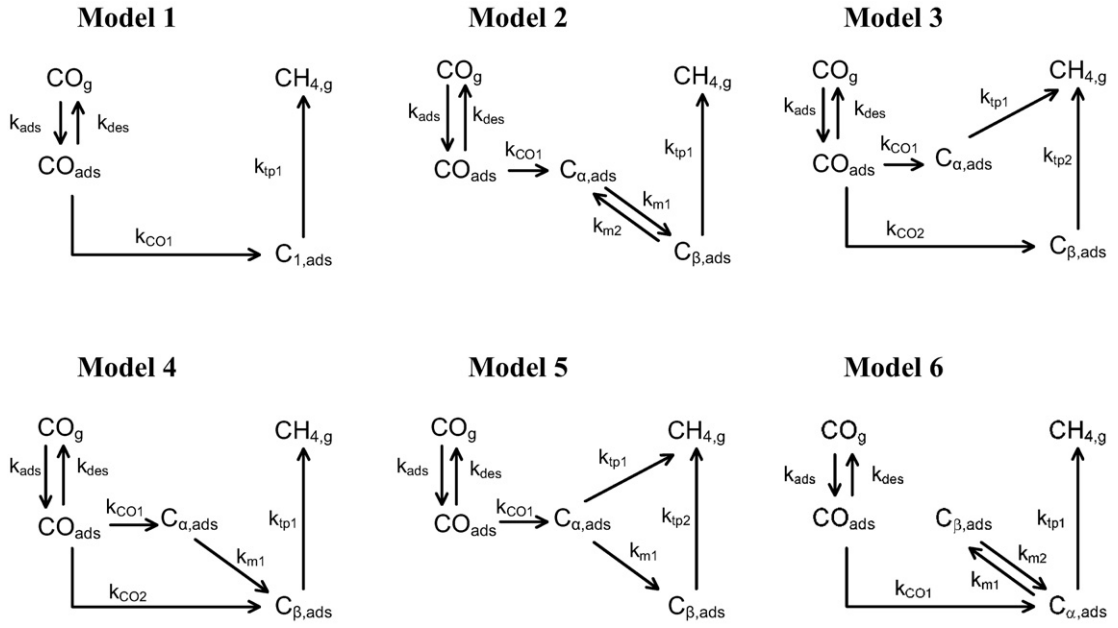

Fig. 6. Schematic representation of the six methanation models based on CO and CH_4 in the gas phase and CO_{ads}, C_α and C_β as the surface components.

Table 1
Optimised parameter estimates for the methanation reaction according to the models in Fig. 6. The surface concentration of CO_{ads} and the gas phase concentration of CH_4 are the model predictions using the corresponding optimal parameter estimates.[a]

	Model 1	Model 2	Model 3	Model 4	Model 5	Model 6
k_{CO1}	$6.24 \times 10^{-1} \pm 2.9 \times 10^{-2}$	$1.40 \pm 2.4 \times 10^{-1}$	$5.26 \times 10^{-1} \pm 1.6 \times 10^{-2}$	$4.85 \times 10^{-1} \pm 12.74$	$6.49 \times 10^{-1} \pm 2.9 \times 10^{-2}$	$6.26 \times 10^{-1} \pm 2.9 \times 10^{-2}$
k_{CO2}			$1.25 \times 10^{-1} \pm 1.6 \times 10^{-2}$	$1.51 \times 10^{-1} \pm 12.73$		
k_{m1}		$1.62 \times 10^{-1} \pm 5.4 \times 10^{-2}$		2.29 ± 237	$1.29 \times 10^{-2} \pm 2.2 \times 10^{-3}$	$2.57 \times 10^{-2} \pm 3.6 \times 10^{-3}$
k_{m2}		$9.8 \times 10^{-2} \pm 6.3 \times 10^{-3}$				$2.40 \times 10^{-3} \pm 3.0 \times 10^{-4}$
k_{tp1}	$9.10 \times 10^{-3} \pm 8.0 \times 10^{-4}$	$8.40 \times 10^{-3} \pm 3.0 \times 10^{-3}$	$1.97 \times 10^{-2} \pm 2.4 \times 10^{-3}$	$9.40 \times 10^{-3} \pm 1.0 \times 10^{-3}$	$1.49 \times 10^{-2} \pm 1.4 \times 10^{-3}$	$1.34 \times 10^{-2} \pm 1.3 \times 10^{-3}$
k_{tp2}			$1.90 \times 10^{-3} \pm 2.0 \times 10^{-4}$		$1.60 \times 10^{-3} \pm 1.0 \times 10^{-4}$	
χ^{2b}	1243	1652	1652	1652	1652	1652
WR[c]	4084	3856	455	2456	436	2070
L_{CO}	$2.80 \times 10^{-4} \pm 1 \times 10^{-5}$	$2.34 \times 10^{-4} \pm 1 \times 10^{-5}$	$2.79 \times 10^{-4} \pm 1 \times 10^{-5}$	$2.80 \times 10^{-4} \pm 1 \times 10^{-5}$	$2.91 \times 10^{-4} \pm 1 \times 10^{-5}$	$2.87 \times 10^{-4} \pm 1 \times 10^{-5}$
$CH_{4,ss}$	$1.76 \times 10^{-3} \pm 2 \times 10^{-4}$	$6.17 \times 10^{-4} \pm 2 \times 10^{-4}$	$1.96 \times 10^{-3} \pm 2 \times 10^{-4}$	$1.80 \times 10^{-3} \pm 2 \times 10^{-4}$	$1.90 \times 10^{-3} \pm 2 \times 10^{-4}$	$1.70 \times 10^{-3} \pm 2 \times 10^{-4}$

[a] Units: all k's in (s^{-1}), L_{CO} in ($mol\,kg_{cat}^{-1}$) and $CH_{4,ss}$ in ($mol\,m_g^{-3}$).

[b] χ^2 is the 95% chi-squared value obtained from the parameter estimation results.

[c] WR is the weighted residual obtained from the parameter estimation results.

where X_{CO} is the conversion of CO. The mean residence of $C_{1,ads}$ was ca. 1000 s which resulted in a surface concentration of 0.08 $mol\,kg^{-1}$ (or 0.2 ML) for the total $C_{1,ads}$ species. This higher surface coverage of $C_{1,ads}$ than of CO_{ads} on our Fe catalyst is different to all other FT metals (see introduction). This is consistent with recent kinetic modelling. Botes and Breman [43] have shown that at commercially relevant conditions, the reaction order for CO on the iron-based is positive whilst for the cobalt-based catalyst it is negative. This implies that the CO coverage on the iron-based catalyst is lower than for the cobalt-based catalyst.

3.3. Model identification and discrimination

Based on two gas phase components (CO and CH_4) and three surface species components (CO_{ads}, $C_{\alpha\,ads}$, $C_{\beta\,ads}$), Van Dijk et al. [20] tested six possible methanation models, shown in Fig. 6. Some of these models have also been used by Happel [34] and Soong et al. [32]. The same set of models was screened in our study using parameter estimation. Apart from model 1, there are six kinetic parameters to be estimated for each model. Our initial efforts showed that some of these parameters are highly correlated. To simplify the parameter estimation process, k_{ads} and k_{des} were fixed. The adsorption/desorption of CO was considered to be a fast reaction and in equilibrium. The consumption of CO_{ads} to form FT products relative to desorption into the gas phase was insignificant for k_{ads} values greater than 0.07 $mol\,kg_{cat}^{-1}\,s^{-1}$ resulting in a CO equilibrium constant of 2.6×10^{-3} $mol\,kg_{cat}^{-1}$. So, for modeling purposes any arbitrary value of k_{ads} greater than 0.07 $mol\,kg_{cat}^{-1}\,s^{-1}$ can be chosen and k_{des} can be calculated from the CO equilibrium constant. In this study, the modeling results for a k_{ads} value of 0.1 $mol\,kg_{cat}^{-1}\,s^{-1}$ with a corresponding k_{des} of 38 s^{-1} are presented.

The model predictions for $^{13}CH_4$ obtained using the optimised parameters (in Table 1) are presented in Fig. 7. Methanation models 1, 2, and 4 fail to describe the $^{13}CH_4$ transients, whilst models 3, 5, and 6 give the best fits. A weighted residual value less than the chi-squared value is considered a good fit. In Table 1, the weighted residuals for models 3 and 5 are lower than the chi-squared values indicating a good fit, whereas model 6 has a higher weighted residual, and hence is considered a bad fit. However, all three models predict both the surface concentration of CO_{ads} and the gas phase concentration of CH_4 equally well. So, at this stage of the modeling, we cannot rule out model 6 based only on the weighted residual value. This issue of model identifiability and distinguishibility with this type of modeling has been discussed by Happel [34] and was also reported by Van Dijk et al. [20]. These authors showed that successful further model dis-

crimination is possible if either more experimental data other than from SSITKA is considered, or the models are extended to incorporate the formation of hydrocarbons. An example of the former approach could be quantification of the surface concentrations of C_α and C_β. The latter approach is used in this study.

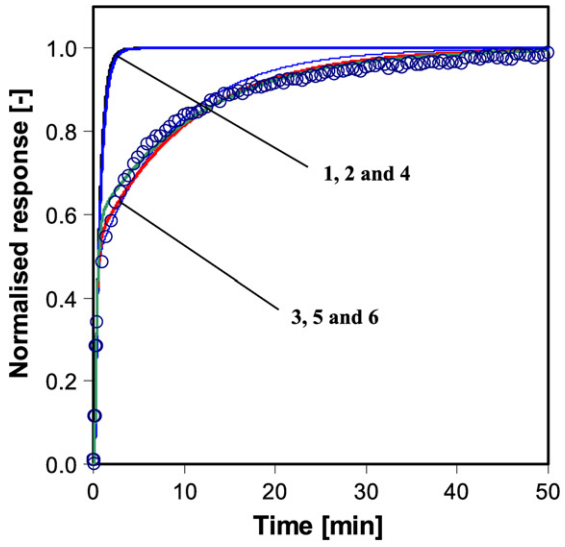

Fig. 7. Model predictions for the $^{13}CH_4$ transients for the methanation models shown in Fig. 6. The symbols (○) are $^{13}CH_4$ data points obtained at $H_2/CO = 15$, 330 °C, 1.2 bar, and GHSV = 7412 ml h^{-1} g_{cat}^{-1} and the solid lines are the model predictions.

3.4. Parameter quantification

The methanation models 3, 5, and 6 (in Fig. 6) can describe our methanation results better than the other three models. These models are thus suitable to extend towards the formation of the higher hydrocarbon Fischer–Tropsch products, and by doing so, the parameters for the methanation models can be quantified. Both chain-growth and chain-initiation need to be considered when modeling the Fischer–Tropsch synthesis. The latter reaction is not considered in full as this will require modeling the transients of the higher hydrocarbons which is not in the scope of this paper. However, the formation of the higher hydrocarbons from C_α and C_β is included in our modeling as a net consumption rate [44]. Chain-initiation involves C–C coupling reactions and is included in the models via the combination of: (1) two C_α species, (2) one C_α and one C_β species, and (3) two C_β species, as shown in Fig. 8 for models 3, 5 and 6. Model 3 is considered symmetrical since the C_α and C_β are interchangeable. In other words, the results for the reaction of two C_α species will be the same as for two C_β species reacting. Hence only two combinations are considered for model 3.

In Table 2, the parameter estimation results for all the models in Fig. 8 are presented and the model descriptions of $^{13}CH_4$ according to the optimised parameters are shown in Fig. 9. Model 5.3 is discarded because it could not describe the methane and

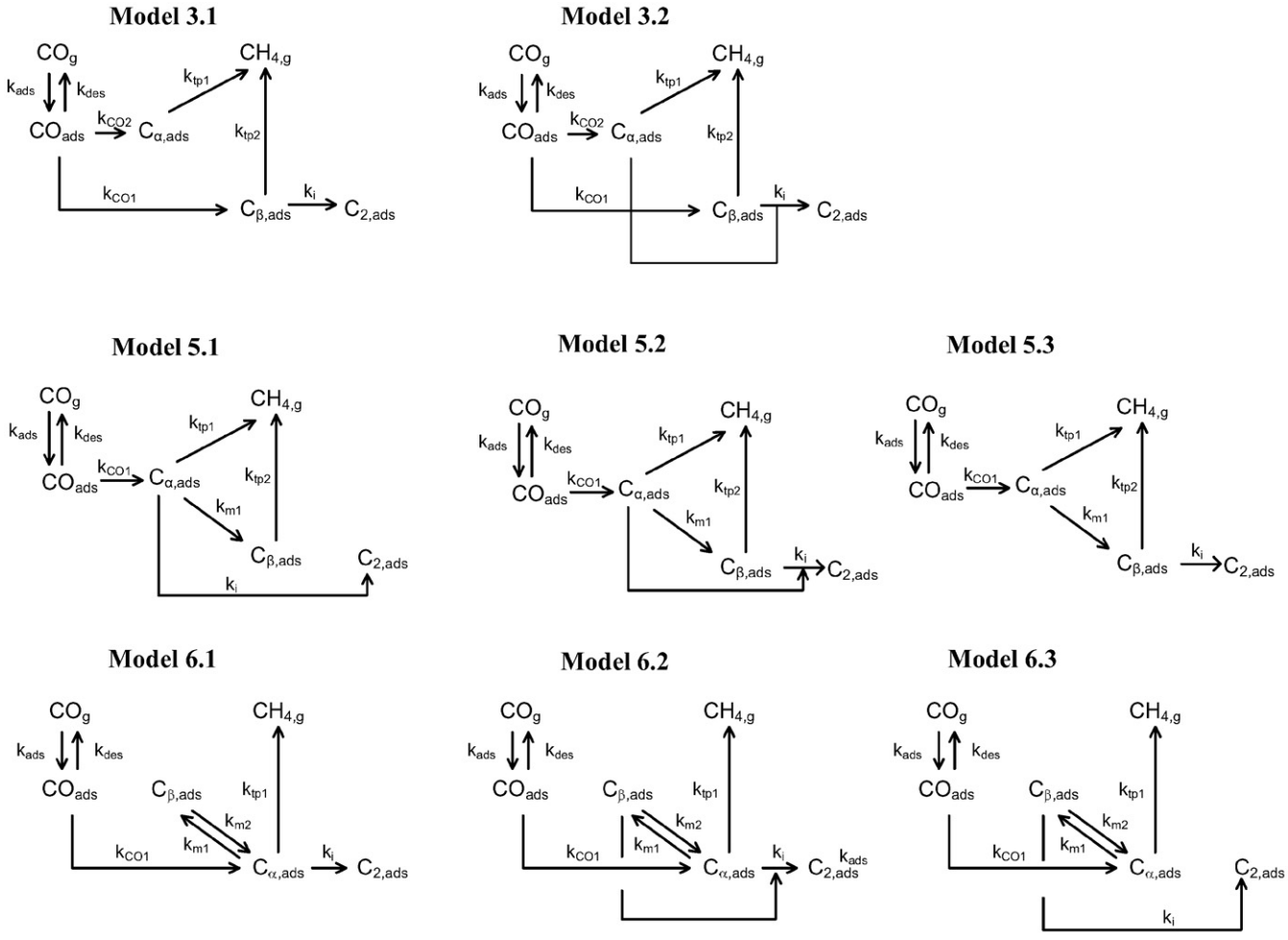

Fig. 8. Schematic representation of the models for the Fischer–Tropsch reaction taking into account different chain initiation pathways based on the three indistinguishable methanation models in Fig. 6.

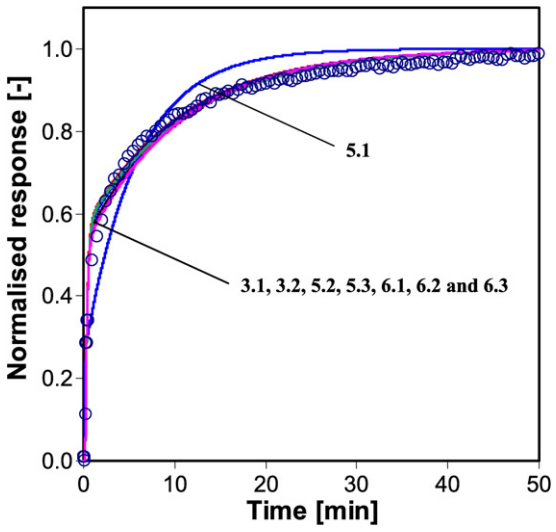

Fig. 9. Model predictions for the $^{13}CH_4$ transients for the models in Fig. 8. The symbols (○) are $^{13}CH_4$ data points obtained at $H_2/CO = 15$, 330 °C, 1.2 bar, and GHSV = 7412 ml h^{-1} g_{cat}^{-1}, and the solid lines are the model predictions.

also failed to predict the steady-state surface and gas phase concentrations. Both combinations of chain-initiation for model 3 can describe the methane transient and both models give good fits according to their weighted residuals. However, model 3.1 predicts a lower $C_{1,tot}$ coverage (0.07 ML) compared to model 3.2 (0.16 ML). On the basis that our experimental value for $C_{1,tot}$ is ca. 0.2 ML, model 3.1 is discarded. Models 5.1, 6.1 and 6.2 are also discarded for the same reason of predicting a low $C_{1,tot}$ coverage. For the methanation model 5, the combination of C_α and C_β (model 5.2) can describe the methane transient with a good fit (see Table 2). The predicted surface and gas phase concentrations for this model are similar to model 3.2 and cannot be further distinguished. Lastly, model 6.3 could describe both surface concentrations adequately but the rate of the C–C coupling reaction, k_i, was not statistically significant. In fact, k_i was poorly estimated in all combinations for the methanation model 6 (models 6.1, 6.2 and 6.3). The buffer step in this model seems to play a significant role in the parameter estimation. The rates constants for this buffer step (k_{m1} and k_{m2}) seem to fluctuate to match the desired surface and gas-phase concentrations without adequately accounting for the C–C coupling reactions. Methanation model 6 is a suitable candidate for describing the methanation results alone but it is inconceivable that this model can be extended to account for the Fischer–Tropsch process. Hence these models (6.1, 6.2 and 6.3) are all discarded.

Finally, the rates of the surface reactions for the models 3.2 and 5.2 are compared to obtain more insight. The rate of CO dissociation, k_{CO1} for model 5.2 and ($k_{CO1} + k_{CO2}$) for model 3.2, is 0.8–0.9 s^{-1}, with k_{CO1} equivalent to k_{CO2} in model 3.2. This rate is two times higher than that reported by Van Dijk [44] for the Co-based catalyst, suggesting that CO dissociates easier on Fe and Co catalysts which is consistent with the study reported by Vannice [45]. Both models have similar termination rate constants with termination from the C_β pool being the rate determining step (25–50 less active for methanation). No further model discrimination between these two models is possible based on the available experimental data.

In summary, models 3.2 and 5.2 both give the best fits for the methanation transients and predict similar steady-state concentrations of CH_4 in the gas-phase and the surface concentrations of CO_{ads}, C_α, and C_β. Both these models have two pathways towards the formation of methane. In model 3.2 these pathways are independent whereas in model 5.2, the C_α and C_β pools are in-

Table 2
Optimised parameter estimates for the methanation reaction according to the models in Fig. 8. The surface concentrations of CO_{ads}, C_α, and C_β, and the gas phase concentration of CH_4 are the model predictions using the corresponding optimal parameter estimates. Italic values are insignificant parameter estimates.[a]

	Model 3.1	Model 3.2	Model 5.1	Model 5.2	Model 5.3	Model 6.1	Model 6.2	Model 6.3
k_{CO1}	$3.63 \times 10^{-1} \pm 2.3 \times 10^{-1}$	$3.38 \times 10^{-1} \pm 1.2 \times 10^{-1}$	$3.82 \times 10^{-1} \pm 2.3 \times 10^{-1}$	$6.37 \times 10^{-1} \pm 2.4 \times 10^{-1}$	$2.60 \times 10^{-1} \pm 2.25 \times 10^{-1}$	$3.22 \times 10^{-1} \pm 2.3 \times 10^{-1}$	$3.15 \times 10^{-1} \pm 2.3 \times 10^{-1}$	$3.29 \times 10^{-1} \pm 2.3 \times 10^{-1}$
k_{CO2}	$1.16 \times 10^{-1} \pm 1.3 \times 10^{-2}$	$2.39 \times 10^{-1} \pm 1.2 \times 10^{-1}$	–	–	–	–	–	
k_{m1}	–	–	$3.10 \times 10^{-2} \pm 1.9 \times 10^{-2}$	$2.95 \times 10^{-2} \pm 3.2 \times 10^{-3}$	$2.76 \times 10^{-1} \pm 3.63 \times 10^{-2}$	$2.40 \times 10^{-2} \pm 3.3 \times 10^{-3}$	$2.77 \times 10^{-1} \pm 1.4 \times 10^{-2}$	$4.22 \times 10^{-2} \pm 1.9 \times 10^{-2}$
k_{m2}	–	–	–	–	–	$2.26 \times 10^{-3} \pm 2.7 \times 10^{-4}$	$2.59 \times 10^{-3} \pm 1.3 \times 10^{-3}$	$1.93 \times 10^{-3} \pm 9.0 \times 10^{-4}$
k_{tp1}	$2.74 \times 10^{-2} \pm 1.7 \times 10^{-3}$	$2.78 \times 10^{-2} \pm 9.9 \times 10^{-3}$	$3.11 \times 10^{-2} \pm 1.9 \times 10^{-2}$	$1.59 \times 10^{-2} \pm 5.9 \times 10^{-3}$	$1.55 \times 10^{-2} \pm 1.6 \times 10^{-2}$	$2.76 \times 10^{-2} \pm 1.9 \times 10^{-2}$	$2.79 \times 10^{-2} \pm 2.0 \times 10^{-2}$	$2.69 \times 10^{-2} \pm 1.9 \times 10^{-2}$
k_{tp2}	$1.47 \times 10^{-3} \pm 7.3 \times 10^{-5}$	$7.69 \times 10^{-4} \pm 3.8 \times 10^{-4}$	$1.8 \times 10^{-3} \pm 8.5 \times 10^{-5}$	$6.61 \times 10^{-4} \pm 3.0 \times 10^{-4}$	$3.02 \times 10^{-4} \pm 3.3 \times 10^{-4}$	–	–	–
k_i	*8.24 ± 5.31*	*$8.33 \times 10^{-1} \pm 1.4 \times 10^{-1}$*	*3.27 ± 21.8*	*$4.23 \times 10^{-1} \pm 5.16 \times 10^{-2}$*	*$2.85 \times 10^{-2} \pm 4.9 \times 10^{-3}$*	*$1.60 \times 10^{-4} \pm 6.52$*	*$1.05 \times 10^{-3} \pm 6.6 \times 10^{-1}$*	*$2.40 \times 10^{-3} \pm 2.4 \times 10^{-2}$*
χ^2[b]	1651	1651	1651	1651	1651	1651	1651	1651
WR[c]	1437	1448	1480	1411	2314	2084	2075	2074
L_{CO}	$2.34 \times 10^{-4} \pm 1 \times 10^{-5}$	$2.31 \times 10^{-4} \pm 1 \times 10^{-5}$	$2.36 \times 10^{-4} \pm 1 \times 10^{-5}$	$2.30 \times 10^{-4} \pm 1 \times 10^{-5}$	$2.40 \times 10^{-4} \pm 1 \times 10^{-5}$	$2.38 \times 10^{-4} \pm 1 \times 10^{-5}$	$2.38 \times 10^{-4} \pm 1 \times 10^{-5}$	$2.38 \times 10^{-4} \pm 1 \times 10^{-5}$
L_{C_α}	1.30×10^{-3}	1.01×10^{-3}	1.01×10^{-3}	2.02×10^{-3}	2.14×10^{-4}	1.99×10^{-3}	1.91×10^{-3}	1.95×10^{-3}
L_{C_β}	1.82×10^{-2}	3.40×10^{-2}	1.72×10^{-2}	3.89×10^{-2}	2.32×10^{-2}	2.06×10^{-2}	2.04×10^{-2}	2.96×10^{-2}
$L_{C_{1,tot}}$	1.90×10^{-2}	6.94×10^{-2}	2.52×10^{-2}	6.11×10^{-2}	1.21×10^{-1}	2.86×10^{-2}	3.06×10^{-2}	5.84×10^{-2}
θ_{CO}	0.0009	0.0009	0.0009	0.0009	0.0009	0.0009	0.0009	0.0009
$\theta_{C_{1,tot}}$	0.07	0.13	0.07	0.16	0.09	0.09	0.08	0.12
$CH_{4,ss}$	2.30×10^{-3}	2.12×10^{-3}	3.56×10^{-3}	1.99×10^{-3}	2.09×10^{-3}	2.92×10^{-3}	2.87×10^{-3}	2.67×10^{-3}

[a] Units: all k's in (s^{-1}) except k_i in (kg_{cat} mol^{-1} s^{-1}), L_{CO} in (mol kg_{cat}^{-1}) and $CH_{4,ss}$ in (mol m_g^{-3}).
[b] χ^2 is the 95% chi-squared value obtained from the parameter estimation results.
[c] WR is the weighted residual obtained from the parameter estimation results.

terlinked. Chain-initiation involves the combination of both these carbon pools.

4. Conclusions

Experimental observations obtained using a $^{12}CO \rightarrow {}^{13}CO$ transient switch indicated that molecularly adsorbed CO on the Fe/K catalyst is extremely low, ca. 9×10^{-4} ML, whilst the $C_{1,tot}$ is much higher, 0.25 ML. For the methanation reactions, the parameter estimation study showed that three models are indistinguishable. All these models have a buffer step or parallel route towards the formation of methane. The chain initiation reaction (C–C coupling) was included which resulted in eight models being tested. The results showed that two models remain indistinguishable. Both these models have two surface intermediates (C_α and C_β) active towards methanation and higher hydrocarbon formation. The quantification of the kinetic rate parameters was performed by accounting for the higher hydrocarbon formation. The results showed that C_β is the larger pool, occupying 92% of the $C_{1,tot}$ coverage and is 25–50 less active for methanation than C_α. The chain-initiation reaction (C–C coupling) involves a combination of C_α and C_β to form the C_2 surface intermediate.

Acknowledgments

The authors gratefully acknowledge the financial support of Sasol Technology, R&D Division and the Netherlands Organisation for Scientific Research (NWO).

References

[1] M.E. Dry, Appl. Catal. A 138 (1996) 319.
[2] M.E. Dry, Catal. Today 71 (2002) 227.
[3] A.P. Steynberg, R.L. Espinoza, B. Jager, A.C. Vosloo, Appl. Catal. A 186 (1999) 41.
[4] R.L. Espinoza, A.P. Steynberg, B. Jager, A.C. Vosloo, Appl. Catal. A 186 (1999) 13.
[5] A.P. Steynberg, Stud. Surf. Sci. Catal. 152 (2004) 1.
[6] J. Happel, Chem. Eng. Sci. 33 (1978) 1567.
[7] C.O. Bennett, Am. Chem. Soc. Symp. Ser. (1982) 1.
[8] P. Biloen, J. Mol. Catal. 21 (1983) 17.
[9] S.L. Shannon, J. Goodwin, Chem. Rev. 95 (1995) 677.
[10] J. Galuszka, T. Sano, J.A. Sawicki, J. Catal. 136 (1992) 96.
[11] J. Xu, C.H. Bartholomew, J. Phys. Chem. B 109 (2005) 2392.
[12] A.M. Efstathiou, C.O. Bennett, Chem. Eng. Commun. 83 (1989) 129.
[13] A.M. Efstathiou, T. Chafik, D. Bianchi, C.O. Bennett, J. Catal. 147 (1994) 24.
[14] A.M. Efstathiou, C.O. Bennett, J. Catal. 120 (1989) 118.
[15] A.M. Efstathiou, C.O. Bennett, J. Catal. 120 (1989) 137.
[16] A.M. Efstathiou, J. Mol. Catal. 69 (1991) 41.
[17] J.H. Siddall, M.L. Miller, W.N. Delgass, Chem. Eng. Commun. 83 (1989) 261.
[18] M. Agnelli, H.M. Swaan, C. Marquez-Alvarez, G.A. Martin, C. Mirodatos, J. Catal. 175 (1998) 117.
[19] I.G. Bajusz, J. Goodwin, J. Catal. 169 (1997) 157.
[20] H.A.J. Van Dijk, J.H.B.J. Hoebink, J.C. Schouten, Top. Catal. 26 (2003) 111.
[21] C.A. Mims, L.E. McCandish, J. Am. Chem. Soc. 107 (1985) 696.
[22] C.A. Mims, L.E. McCandish, J. Phys. Chem. 91 (1987) 929.
[23] D.M. Stockwell, D. Bianchi, C.O. Bennett, J. Catal. 113 (1988) 13.
[24] M.W. Balakos, S.S.C. Chuang, G. Srinivas, M.A. Brundage, J. Catal. 157 (1995) 51.
[25] D.M. Stockwell, J.S. Chung, C.O. Bennett, J. Catal. 112 (1988) 135.
[26] C. Marquez-Alvarez, G.A. Martin, C. Mirodatos, in: A. Parmaliana (Ed.), Proc. 5th Int. Natural Gas Conversion Symposium, in: Stud. Surf. Sci. Catal., vol. V, Elsevier, Amsterdam, 1998, p. 155.
[27] J. Happel, H.Y. Cheh, M. Otarod, S. Ozawa, A.J. Severdia, T. Yoshida, V. Fthenakis, J. Catal. 75 (1982) 314.
[28] K.R. Krishna, A.T. Bell, J. Catal. 139 (1993) 104.
[29] J. Happel, I. Suzuki, P. Kokayeff, V. Fthenakis, J. Catal. 65 (1980) 59.
[30] M. Otarod, S. Ozawa, F. Yin, M. Chew, H.Y. Cheh, J. Happel, J. Catal. 84 (1983) 156.
[31] M. Otarod, J. Happel, E. Walter, Appl. Catal. A 160 (1997) 3.
[32] Y. Soong, K. Krishna, P. Biloen, J. Catal. 97 (1986) 330.
[33] R.L. Espinoza, T.C. Bromfield, F.G. Botes, J.L. Visagie, K.H. Lawson, P. Gibson, US Patent 6844370 (2005), to Sasol Technology (Pty) Ltd.
[34] J. Happel, Isotopic Assessment of Heterogeneous Reactors, Academic Press, New York, 1986.
[35] C.O. Bennett, in: A.T. Bell, L.L. Hegedus (Eds.), Catalysis under Transient Conditions, Am. Chem. Soc., Washington, DC, 1982, p. 1.
[36] gPROMS Advanced User Guide, Process Systems Enterprise, 2004, p. 37.
[37] M.E. Dry, in: R.B. Anderson, M. Boudart (Eds.), in: Catalysis Science and Technology, vol. 15-255, Springer-Verlag, Berlin, 1981, p. 1.
[38] H.E. du Plessis, Ph.D. thesis, University of Johannesburg, South Africa, 2007.
[39] P. Biloen, J.N. Helle, F.G.A. van den Berg, W.M.H. Sachtler, J. Catal. 81 (1983) 450.
[40] K. Sudsakorn, J. Goodwin, A.A. Adeyiga, J. Catal. 213 (2003) 204.
[41] D. Bianchi, S. Borcar, F. Teule-Gay, C.O. Bennett, J. Catal. 82 (1983) 442.
[42] M. Boudart, A. Delbouille, J.A. Dumesic, S. Khammouma, H. Topsoe, J. Catal. 37 (1975) 486.
[43] F.G. Botes, Catal. Rev. Sci. Eng. (2008), DOI: 10.1080/01614940802477250, in press.
[44] H.A.J. Van Dijk, A mechanistic study using transient isotopic tracing, Ph.D. thesis, 2001, Technische Universiteit Eindhoven, Eindhoven, the Netherlands, http://alexandria.tue.nl/extra2/200111083.pdf.
[45] M.A. Vannice, J. Catal. 37 (1975) 462.